Am J Transl Res 2026;18(5):4474-4491
www.ajtr.org /ISSN:1943-8141/AJTR0172855

Original Article

TRIM62 promotes osteoarthritis progression by facilitating GPX4 ubiquitination and chondrocyte ferroptosis

Xiaobin Chen[1], Yonghong Zhang[2]

[1]*Second Clinical Medical College, Shanxi Medical University, Taiyuan 030001, Shanxi, China;* [2]*Department of Orthopaedics, Second Hospital of Shanxi Medical University, Taiyuan 030001, Shanxi, China*

Received March 24, 2026; Accepted May 6, 2026; Epub May 15, 2026; Published May 30, 2026

Abstract: Objectives: This study investigates the role of Tripartite motif containing 62 (TRIM62) in osteoarthritis (OA) progression, focusing on its regulation of Glutathione Peroxidase 4 (GPX4) ubiquitination and chondrocyte ferroptosis. Methods: An OA rat model was established via anterior cruciate ligament transection (ACLT) and then primary chondrocytes were stimulated with interleukin-1β (IL-1β) in vitro. TRIM62 expression was manipulated using short hairpin RNA (shRNA) or overexpression plasmids. Ferroptosis was assessed by measuring GPX4, solute carrier family 7 member 11 (SLC7A11), glutathione (GSH), reactive oxygen species (ROS), ferrous iron (Fe^{2+}), and mitochondrial membrane potential. Protein interactions were evaluated by co-immunoprecipitation (Co-IP). Results: RIM62 expression was significantly increased in osteoarthritic cartilage and in chondrocytes treated with IL-1β. TRIM62 knockdown restored GPX4 and collagen type II (COL II) expression, reduced disintegrin and metalloproteinase with thrombospondin motifs 5 (ADAMTS5) levels, suppressed ferroptosis, and alleviated cartilage damage *in vivo*. Conversely, TRIM62 overexpression exacerbated chondrocyte injury and ferroptosis, effects specifically reversed by ferrostatin-1 (Fer-1). Mechanistically, TRIM62 directly interacted with GPX4 and promoted its proteasomal degradation. Conclusions: TRIM62 facilitates OA progression by inducing GPX4 ubiquitination and degradation, thereby promoting chondrocyte ferroptosis. The TRIM62-GPX4-ferroptosis axis represents a promising therapeutic target for OA.

Keywords: Osteoarthritis, tripartite motif containing 62, glutathione peroxidase 4, ferroptosis

Introduction

Osteoarthritis (OA) is among the most prevalent degenerative joint disorders globally, affecting more than 500 million individuals and placing significant socioeconomic burdens on healthcare systems. The disease results in progressive cartilage degradation, alterations in the underlying bone, inflammation of the synovial lining, and the formation of bone spurs. These pathological changes contribute to joint pain, stiffness, and impaired mobility [1, 2]. Despite decades of research, the molecular mechanisms underlying OA remain unclear. No effective therapies exist to alter disease progression [2-4]. Chondrocytes are the only cells in articular cartilage. They maintain a balance between building up and breaking down the extracellular matrix (ECM) [5, 6]. Under pathological conditions, chondrocytes undergo phenotypic alterations and various forms of cell death, contributing to cartilage degeneration and OA progression [6, 7].

Ferroptosis is a newly discovered type of regulated cell death, characterized by the accumulation of iron-driven lipid peroxides and striking changes in cell structure, such as shrunken mitochondria and denser membranes [8, 9]. Unlike apoptosis and necroptosis, ferroptosis is driven by glutathione (GSH) depletion and the inactivation of glutathione proxidase 4 (GPX4), leading to uncontrolled lipid peroxidation and subsequent membrane damage [10, 11]. Pathological stimuli prevalent in OA, such as mechanical overloading and pro-inflammatory cytokines, can induce intracellular iron accumulation. Excessive iron can trigger the Fenton reaction, thereby increasing the production of reactive oxygen species (ROS), leading to lipid peroxidation of the cartilage cell membrane [12]. Importantly, the impact of ferroptosis in

https://doi.org/10.62347/DKML5977

OA is not limited to simple cell loss; it also plays a critical role in disrupting ECM homeostasis [13, 14]. Ferroptosis-prone chondrocytes exhibit increased expression of matrix-degrading enzymes alongside reduced synthesis of collagen type II (COL II) and proteoglycans. This transition to a catabolic state accelerates the structural collapse of articular cartilage [14]. Furthermore, ferroptosis-induced cell damage can further exacerbate synovial inflammation, establishing a vicious cycle of joint destruction. For example, iron levels in the synovial fluid of OA patients are significantly elevated, and marked iron deposition is also observed in synovial tissue [15]. Under conditions of iron overload, synovial macrophages polarize into the M1 phenotype, leading to the production of the inflammatory factors. These factors trigger further inflammatory responses in the synovium, promoting cartilage destruction and osteophyte formation, ultimately aggravating the progression of osteoarthritis [15, 16].

GPX4 plays a key role in protecting cells from ferroptosis. It does this by turning harmful lipid hydroperoxides into harmless lipid alcohols, which stops the spread of damaging lipid peroxidation [1]. The cystine/glutamate antiporter system Xc-, comprising solute carrier family 7 member 11 (SLC7A11) and solute carrier family 3 member 2 (SLC3A2) subunits, provides cysteine for GSH biosynthesis, which acts as an essential cofactor for GPX4 enzymatic activity [15, 17]. Downregulation or inactivation of GPX4 renders cells highly susceptible to ferroptotic cell death [18]. Conditional knockout of GPX4 in murine chondrocytes has been shown to exacerbate experimental OA, whereas supplementation with the ferroptosis suppressor protein-1 (FSP1) and coenzyme Q10 partially rescues the phenotype [19, 20]. The results highlight the essential function of GPX4 in safeguarding chondrocytes against ferroptosis and preserving cartilage integrity. Post-translational modifications, particularly ubiquitination, represent a crucial regulatory mechanism governing protein stability and function [20]. E3 ubiquitin ligases catalyze the transfer of ubiquitin molecules to target proteins, typically marking them for proteasomal degradation [21, 22]. The tripartite motif-containing (TRIM) protein family represents a large group of RING-type E3 ubiquitin ligases that participate in various cellular processes, such as innate immunity, autophagy, and carcinogenesis [23, 24]. Emerging evidence indicates that multiple TRIM family members regulate ferroptosis by ubiquitinating key ferroptotic regulators [24, 25]. For instance, TRIM26 has been shown to catalyze K63-linked ubiquitination of GPX4, thereby stabilizing GPX4 and suppressing ferroptosis in glioma cells [26]. On the contrary, TRIM25 is capable of mediating the K48-linked ubiquitination degradation of GPX4 and enhancing the ferroptosis process in pancreatic cancer cells [27]. TRIM7 has been reported to facilitate ferroptosis in gastric cancer through K48-linked ubiquitination and degradation of SLC7A11 [27]. These studies highlight the context-dependent roles of TRIM proteins in modulating ferroptosis sensitivity. TRIM62, a member of the TRIM subfamily, functions as an E3 ubiquitin ligase implicated in innate immunity, inflammation, and tumorigenesis [28, 29]. Recent investigations have demonstrated that TRIM62 promotes GPX4 ubiquitination and degradation, thereby aggravating ferroptosis in ischemic stroke models [30]. However, whether TRIM62 participates in OA pathogenesis and whether it regulates chondrocyte ferroptosis through modulating GPX4 stability remains entirely unexplored. Given the established role of ferroptosis in OA and the emerging function of TRIM62 in regulating GPX4, we hypothesized that TRIM62 might contribute to OA progression by promoting GPX4 ubiquitination and subsequent chondrocyte ferroptosis. In this study, we examined how TRIM62 is expressed in OA cartilage, explored its role in chondrocyte ferroptosis and cartilage degeneration, and investigated how TRIM62 regulates GPX4. Our results may offer new insights into OA development and suggest that TRIM62 could be a target for OA treatment.

Materials and methods

Ethical statement

All animal experiments were approved by the Animal Ethics Committee of Second Hospital of Shanxi Medical University and conducted in accordance with the National Institutes of Health Guidelines for the Care and Use of Laboratory Animals, as well as the ethical principles outlined in the Declaration of Helsinki (1964) and its subsequent amendments

Animals and OA model establishment

Male Sprague-Dawley (SD) rats, aged 8 weeks and weighing 200-220 g (specific pathogen-

free grade), were obtained from Huafukang Biotechnology (Beijing, China). The animals were maintained under controlled environmental conditions (22-24°C, 50-60% humidity, 12-hour light/dark cycle) with ad libitum access to food and water.

The OA model was created by cutting the anterior cruciate ligament (ACL) as described in earlier studies. Rats were anesthetized with 1% pentobarbital sodium (40 mg/kg, Sigma-Aldrich, St. Louis, MO, USA) given by intraperitoneal injection. Once anesthetized, each rat was placed on its back, and the knee joint was exposed using a medial parapatellar approach. The anterior cruciate ligament was then cut with microsurgical scissors. In the sham group, the knee joint was exposed, but the ligament was not cut. After surgery, the incision was closed in layers, and rats were given meloxicam (1 mg/kg, subcutaneously) for pain relief for 3 days.

For *in vivo* knockdown experiments, sh-TRIM62 lentivirus or sh-NC lentivirus (1×10^8 TU/mL, 50 μL; GeneChem, Shanghai, China) was injected into the knee joint cavity immediately after surgery and once weekly for 4 weeks. Rats were sacrificed by CO_2 asphyxiation 8 weeks post-surgery, and cartilage tissues were harvested for subsequent analyses.

Primary chondrocyte isolation and culture

As mentioned earlier, the primary chondrocytes were first isolated from the articular cartilage of neonatal SD rats (within 5 days after birth). Cartilage tissues were dissected under sterile conditions, minced into approximately 1 mm^3 pieces, and digested with 0.25% trypsin-EDTA (Gibco, Grand Island, NY, USA) for 30 minutes at 37°C. This was followed by digestion with 0.2% type II collagenase (Sigma-Aldrich, St. Louis, MO, USA) for 6 to 8 hours at 37°C. The cell suspension was filtered through a 70 μm cell strainer, centrifuged at 1,000 rpm for 5 min, and resuspended in DMEM/F12 medium (Gibco) supplemented with 10% fetal bovine serum (FBS; Gibco) and 1% penicillin-streptomycin (Gibco). Cells were grown at 37°C in a humidified atmosphere with 5% CO_2. For all experiments, chondrocytes from passages 1-2 were used.

In vitro OA model and cell treatment

To create an in vitro OA model, chondrocytes were exposed to recombinant rat IL-1β (10 ng/mL; PeproTech, Rocky Hill, NJ, USA) for 24 hours. Control cells received the same amount of phosphate-buffered saline (PBS) as a vehicle.

To investigate cell death pathways, several inhibitors sourced from MedChemExpress (Monmouth Junction, NJ, USA) were employed: Ferrostatin-1 (Fer-1, 1 μM) for ferroptosis, Necrostatin-1 (Nec-1, 30 μM) for necroptosis, Z-VAD-FMK (Z-VAD, 20 μM) for pan-caspase inhibition, and MG132 (2.5 μM) for proteasome blocking. These agents were prepared as stock solutions in dimethyl sulfoxide (DMSO; Sigma-Aldrich). The control group was treated with a vehicle (DMSO) of the same volume, ensuring that the concentration of DMSO in the culture environment remained below 0.1% to prevent potential solvent toxicity.

Cell transfection and lentiviral infection

To construct a TRIM62 overexpression model, the complete rat TRIM62 cDNA sequence was integrated into the pcDNA3.1 backbone (GeneChem, Shanghai, China). This recombinant plasmid, designated as TRIM62-OE, was subsequently introduced into chondrocytes. An unmodified pcDNA3.1 vector served as the negative control. These delivery procedures were facilitated by the Lipofectamine 3000 reagent (Invitrogen, Carlsbad, CA, USA) in strict accordance with the supplier's standardized protocol.

To achieve TRIM62 silencing, lentiviral particles carrying either rat-specific shRNA (sh-TRIM62) or a non-targeting control sequence (sh-NC) were procured from GeneChem (Shanghai, China). Chondrocytes were exposed to the virus at an MOI of 20 for a 24-hour period, with 5 μg/mL polybrene (Sigma-Aldrich) added to improve transduction efficiency. The success of the genetic knockdown was subsequently validated 72 hours after infection by assessing TRIM62 protein levels via Western blot.

RNA extraction and RT-qPCR

Isolation of total RNA from either chondrocytes or cartilage specimens was performed using

TRIzol reagent (Invitrogen, Carlsbad, CA, USA), adhering to the standardized steps provided by the supplier. The quantity and quality of the harvested RNA were evaluated using a NanoDrop 2000 spectrophotometer (Thermo Fisher Scientific, Waltham, MA, USA). Subsequently, 1 μg of the purified RNA was reverse-transcribed into complementary DNA (cDNA) with the assistance of a PrimeScript RT Reagent Kit (Takara, Dalian, China).

Quantitative real-time PCR was performed using SYBR Green PCR Master Mix (Takara) on an ABI 7500 Real-Time PCR System (Applied Biosystems, Foster City, CA, USA). The programmed thermal profile included an initial stage at 95°C for 30 s, with 40 subsequent cycles comprising denaturation at 95°C (5 s) and annealing/extension at 60°C (34 s). To evaluate relative mRNA abundance, the $2^{-\Delta\Delta Ct}$ method was applied, utilizing β-actin as the endogenous control for normalization. The following primer pairs were synthesized: TRIM62 forward, 5'-TGGGTGTCTTCCTGGACTATG-3' and reverse, 5'-TTAGATGCGGACCGTGTTG-3'; β-actin forward, 5'-GGAGTCTACTGGCGTCTTCAC-3' and reverse, 5'-ATGAGCCCTTCCACGATGC-3'.

Western blot analysis

We harvested total protein from both tissues and cells by employing RIPA lysis medium (Beyotime), which contained a mixture of protease and phosphatase inhibitors from Roche. After assessing protein concentrations via the BCA method (Beyotime), 30 μg of each protein sample was loaded onto 10-12% polyacrylamide gels for separation. The resulting bands were then moved onto PVDF membranes (Millipore, USA) to prepare for downstream antibody incubation.

Non-specific protein interactions were neutralized by incubating membranes in 5% non-fat milk (prepared in TBST) for 60 min. The membranes were then subjected to overnight hybridization at 4°C with specific primary antibodies against TRIM62 (1:1000, Thermo Fisher), SLC7A11, GPX4, COL II (all 1:1000 from Abcam), ADAMTS5 (1:250, Abcam), and β-actin (1:5000, Abcam). Subsequent to TBST rinsing, secondary antibody incubation (1:5000, Abcam) was carried out at ambient temperature. Immunoreactive bands were visualized using a Bio-Rad ECL kit and a ChemiDoc XRS+ imager, with final quantification performed through ImageJ (Bethesda, MD, USA).

Histological analysis

Following 48 h of fixation in 4% paraformaldehyde, the knee samples were subjected to prolonged decalcification in 10% EDTA for one month. After paraffin embedding, the specimens were cut into 5-μm sections. Standard H&E and SOFG staining techniques were employed to visualize joint architecture. The degree of osteoarthritic progression was independently assessed via the OARSI grading scale by two blinded specialists, ensuring the impartiality of the histological evaluation.

Co-immunoprecipitation (Co-IP) assay

Immunoprecipitation was initiated by incubating 500 μg of inhibitor-supplemented cell lysates with specific primary antibodies (TRIM62, GPX4, or SLC7A11; 2 μg each) at 4°C. For the negative control, a matching amount of normal rabbit IgG (CST, USA) was utilized. Following an overnight rotation, 50 μL of Protein A/G magnetic beads were introduced to the mixture for 2 h to pull down the target complexes. The immunoprecipitated fractions were rinsed three times and subsequently boiled in 2× SDS buffer for protein dissociation. The final samples were subjected to immunoblotting to assess protein-protein associations.

Immunofluorescence staining

Tissue sections underwent deparaffinization and hydration prior to heat-induced antigen retrieval (citrate buffer, pH 6.0). Meanwhile, cell samples were fixed in 4% paraformaldehyde (15 min) and made permeable with 0.3% Triton X-100 (10 min). Non-specific binding was neutralized by treating samples with 5% BSA for 60 min. The samples were then co-incubated with primary antibodies targeting TRIM62 and GPX4 at 4°C for at least 12 h. Following PBS washing, fluorescent secondary antibodies (Alexa Fluor 594 and Alexa Fluor 488, 1:500, Invitrogen) were applied for 1 h at room temperature. A 5-min counterstain with DAPI was used to visualize nuclei. Confocal images were acquired via a Carl Zeiss LSM 800 system.

Cell viability assay

Chondrocyte survival was quantified via the CCK-8 assay (Dojindo, Japan) in accordance

with the provided protocol. Briefly, after seeding cells (5×10^3 cells/well) in 96-well plates and completing the indicated treatments, 10 μL of CCK-8 solution was introduced to the culture environment. After incubating for an additional 2 h at 37°C, the absorbance at 450 nm was recorded on a BioTek Synergy H1 system. The final viability results were normalized against the untreated control.

TUNEL assay

Cellular apoptosis was appraised through a TUNEL assay (Beyotime). Briefly, fixed (4% PFA) and permeabilized chondrocytes were exposed to the enzyme/fluorescein-dUTP mixture for 60 min at 37°C while protected from light. After resolving nuclei with DAPI, images were captured on a Nikon platform (Eclipse Ti2). To ensure statistical significance, the percentage of green-fluorescent apoptotic cells was calculated based on the observation of five arbitrary fields per specimen, providing a representative measure of programmed cell death.

Intracellular Fe^{2+} measurement

Intracellular ferrous iron (Fe^{2+}) availability was quantified using an Iron Assay Kit (#ab83366; Abcam) following the supplier's directives. Briefly, chondrocytes (1×10^6) were collected and subjected to mechanical homogenization. To remove debris, samples underwent centrifugation at 16,000×g for 10 min at 4°C. The obtained supernatant was then reacted with an iron reducer (30 min) and subsequently incubated with an iron probe (1 h, room temperature, dark conditions). A microplate reader (Synergy H1; BioTek) was utilized to measure the resulting optical density at a wavelength of 593 nm.

GSH measurement

Concentrations in tissues and cell lysates were appraised using a commercial ELISA kit (#D751008; Sangon Biotech) following the provided manual. Briefly, after homogenization and the removal of cellular debris via centrifugation, the harvested supernatant was subjected to analysis. Absorbance was measured at 450 nm, and individual GSH levels were calculated by fitting the data to a pre-generated standard curve, ensuring accurate quantification across all samples.

Intracellular ROS detection

To monitor intracellular ROS accumulation, a DCFH-DA fluorescent probe (Beyotime) was employed. Chondrocytes were exposed to 10 μM of the probe for a 20-min period at 37°C, with the incubation performed in a light-shielded environment. To eliminate unbound fluorescent dye, the cells were rinsed three times using culture medium lacking serum. Subsequently, green fluorescent signals were visualized and recorded via a Nikon Eclipse Ti2 microscope. The relative intensity of the fluorescence was then determined using ImageJ software.

Mitochondrial membrane potential (ΔΨm) assessment

Mitochondrial membrane potential was assessed using a JC-1 Mitochondrial Membrane Potential Assay Kit (MedChemExpress). Chondrocytes were incubated with JC-1 staining solution (10 μg/mL) for 20 min at 37°C in the dark. Subsequent to rinsing with the specialized staining buffer, cells were examined via a Nikon Eclipse Ti2 fluorescence microscope. High ΔΨm was identified by the presence of red-fluorescent aggregates (585/590 nm), whereas a loss of potential was indicated by green-fluorescent monomers (514/529 nm). To determine the overall mitochondrial status, the intensity ratio of red fluorescence to green fluorescence was calculated for each treatment group.

Statistical analysis

All data are summarized as mean ± SD based on triplicate independent trials. Statistical processing was implemented through GraphPad Prism 9.0 software. To determine differences between two specific groups, the Student's t-test was utilized. For datasets involving more than two groups, one-way ANOVA coupled with Tukey's post-test was applied to evaluate significance. Statistically significant results were defined by a P-value < 0.05.

Results

TRIM62 overexpression coincides with ferroptosis activation in OA-damaged cartilage

To investigate the potential role of TRIM62 in OA pathogenesis, we established an OA rat

model via ACLT and examined TRIM62 expression in cartilage tissue 8 weeks post-surgery. TRIM62 mRNA levels were markedly upregulated in OA cartilage compared with sham-operated controls ($P < 0.001$; **Figure 1A**). Consistent with this finding, we demonstrated a significant increase in TRIM62 protein expression in the OA group ($P < 0.001$; **Figure 1B**).

Given that TRIM62 has been implicated in ferroptosis regulation in other disease contexts, we next assessed ferroptosis-related markers in OA cartilage. The protein levels of two key ferroptosis defense molecules, SLC7A11 and GPX4, were substantially reduced in OA cartilage compared with controls ($P < 0.001$; **Figure 1B**). Histological examination using H&E and SOFG staining revealed pronounced cartilage degeneration in OA rats, characterized by surface irregularities, proteoglycan loss, and chondrocyte disorganization. Assessment via the OARSI grading system revealed that cartilage degeneration was significantly more severe in the OA cohort than in the healthy control group ($P < 0.001$; **Figure 1C**).

Further characterization of ferroptosis hallmarks showed that GSH levels were markedly decreased in OA cartilage ($P < 0.001$; **Figure 1D**), while intracellular ROS accumulation was substantially elevated, as evidenced by enhanced DCFH-DA fluorescence intensity ($P < 0.001$; **Figure 1E**). Additionally, JC-1 staining demonstrated a marked reduction in the red/green fluorescence ratio in OA tissues, indicating impaired mitochondrial membrane potential ($P < 0.001$; **Figure 1F**). Collectively, these data suggest that TRIM62 upregulation coincides with ferroptosis activation in OA cartilage.

TRIM62 knockdown attenuates IL-1β-induced chondrocyte injury and ferroptosis in vitro

To investigate the potential contribution of TRIM62 to the pathological process of chondrocyte damage, we established an *in vitro* OA mimicry by challenging primary rat chondrocytes with IL-1β. Lentiviral-mediated transduction was utilized to achieve TRIM62 silencing (sh-TRIM62) or provide a negative control (sh-NC) before the cells were subjected to the IL-1β insult. The results confirmed efficient knockdown of TRIM62 in sh-TRIM62-infected cells (**Figure 2A**).

IL-1β treatment induced typical OA-like changes in chondrocytes, including elevated TRIM62 and thrombospondin motif 5 (ADAMTS5) expression, reduced levels of SLC7A11, GPX4, and COL II, as well as morphological alterations characterized by cell shrinkage and loss of the characteristic polygonal shape (**Figure 2A**, **2B**). Notably, TRIM62 knockdown substantially reversed these IL-1β-induced changes. In the OA group, knocking out TRIM62 reversed the expression levels of SLC7A11, GPX4 and COL II, while the level of ADAMTS5 was lower compared to the OA group ($P < 0.001$; **Figure 2A**).

Specifically, CCK-8 analysis illustrated that the targeted knockdown of TRIM62 effectively countered the decline in cell survival triggered by IL-1β exposure ($P < 0.001$; **Figure 2C**) Moreover, the elevated intracellular Fe^{2+} concentration observed in the model group was markedly attenuated by sh-TRIM62 ($P < 0.001$; **Figure 2D**). Visualization via TUNEL staining illustrated that the percentage of apoptotic chondrocytes was markedly suppressed by TRIM62 knockdown, falling from roughly 45% in model cells to less than 10% ($P < 0.001$; **Figure 2E**). These results indicate that suppressing TRIM62 expression effectively mitigates IL-1β-mediated cellular insult and subsequent ferroptosis.

TRIM62 overexpression promotes chondrocyte injury specifically through ferroptosis

To more rigorously define TRIM62's contribution to chondrocyte ferroptosis and to discriminate this pathway from alternative modes of programmed cell death, we conducted overexpression assays in conjunction with specific pharmacological blocking. To determine which death mechanism was dominant, TRIM62-overexpressing chondrocytes were challenged with IL-1β both with and without the addition of selective antagonists, namely Fer-1, Nec-1, or Z-VAD, which specifically counteract ferroptosis, necroptosis, and apoptosis, respectively.

Western blot analysis showed that TRIM62 overexpression in IL-1β-treated cells further decreased SLC7A11, GPX4, and COL II expression while increasing ADAMTS5 levels compared with the model group (**Figure 3A**). Strikingly, co-treatment with Fer-1 largely reversed these changes, restoring the expression of ferroptosis defense proteins and ECM compo-

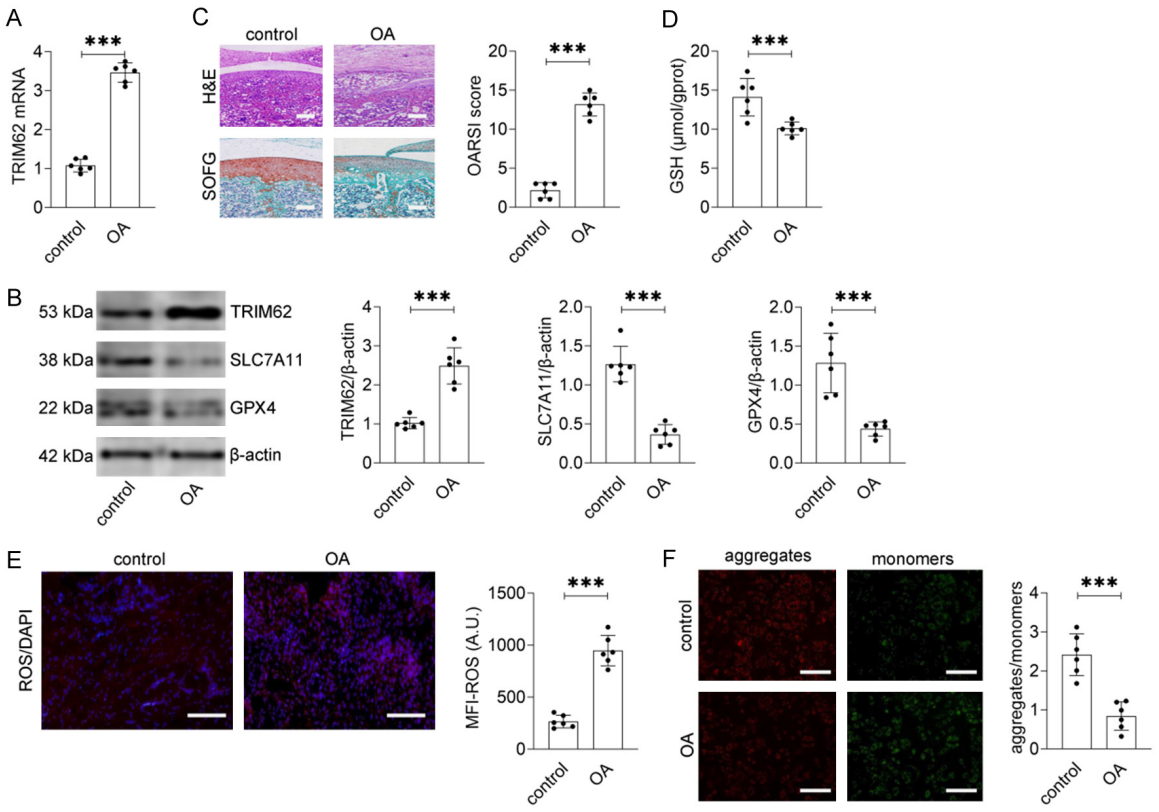

Figure 1. Tripartite motif containing 62 (TRIM62) is upregulated, and ferroptosis is activated in osteoarthritis (OA) cartilage tissues. The OA rat model was established via anterior cruciate ligament transection (ACLT), while control rats underwent sham surgery (n = 6 per group). Cartilage tissues were harvested 8 weeks post-surgery for analysis. A. Relative mRNA expression of TRIM62 was quantified by RT-qPCR. B. Representative Western blot images and quantitative analysis of TRIM62, solute carrier family 7 member 11 (SLC7A11), and glutathione peroxidase 4 (GPX4) protein levels in cartilage tissues. β-actin served as the loading control. C. Histopathological assessment of cartilage damage by hematoxylin and eosin (H&E) staining and safranin O-fast green (SOFG) staining. Cartilage degeneration was evaluated using the OARSI scoring system. D. GSH concentration in cartilage tissues was measured by ELISA. E. ROS levels were detected using the DCFH-DA fluorescent probe. Representative fluorescence images (left) and quantification of mean fluorescence intensity (MFI) (right) are shown. Nuclei were counterstained with DAPI. Scale bar = 100 μm. F. Mitochondrial membrane potential (ΔΨm) was assessed by JC-1 staining. Red fluorescence indicates JC-1 aggregates (high ΔΨm), while green fluorescence represents JC-1 monomers (low ΔΨm). The ratio of aggregates to monomers was calculated and presented in the bar graph. Scale bar = 100 μm. Data are expressed as mean ± SD. ***P < 0.001, connecting lines denote significant differences.

nents. In contrast, neither Nec-1 nor Z-VAD treatment produced comparable effects (**Figure 3A**).

Morphological observations corroborated the Western blot findings. In the model/TRIM62-OE group, chondrocytes presented significant morphological deterioration, characterized by conspicuous cellular contraction. Notably, this damage was exclusively mitigated by the addition of Fer-1, whereas neither Nec-1 nor Z-VAD exerted a protective rescue effect (**Figure 3B**). The CCK-8 assay demonstrated that Fer-1 significantly rescued the reduced cell viability caused by TRIM62 overexpression, whereas Nec-1 and Z-VAD failed to improve cell survival (**Figure 3C**). Similarly, the elevated Fe^{2+} levels in the model/TRIM62-OE group were effectively reduced by Fer-1 treatment but remained unchanged following Nec-1 or Z-VAD administration (**Figure 3D**). TUNEL assay results further confirmed that only Fer-1, and not Nec-1 or Z-VAD, could attenuate the increased cell death induced by TRIM62 overexpression (**Figure 3E**).

Importantly, treatment with Fer-1 alone (model/Fer-1 group) also conferred protection against IL-1β-induced injury, suggesting that ferroptosis represents a major contributor to OA-related chondrocyte damage. Taken together, these

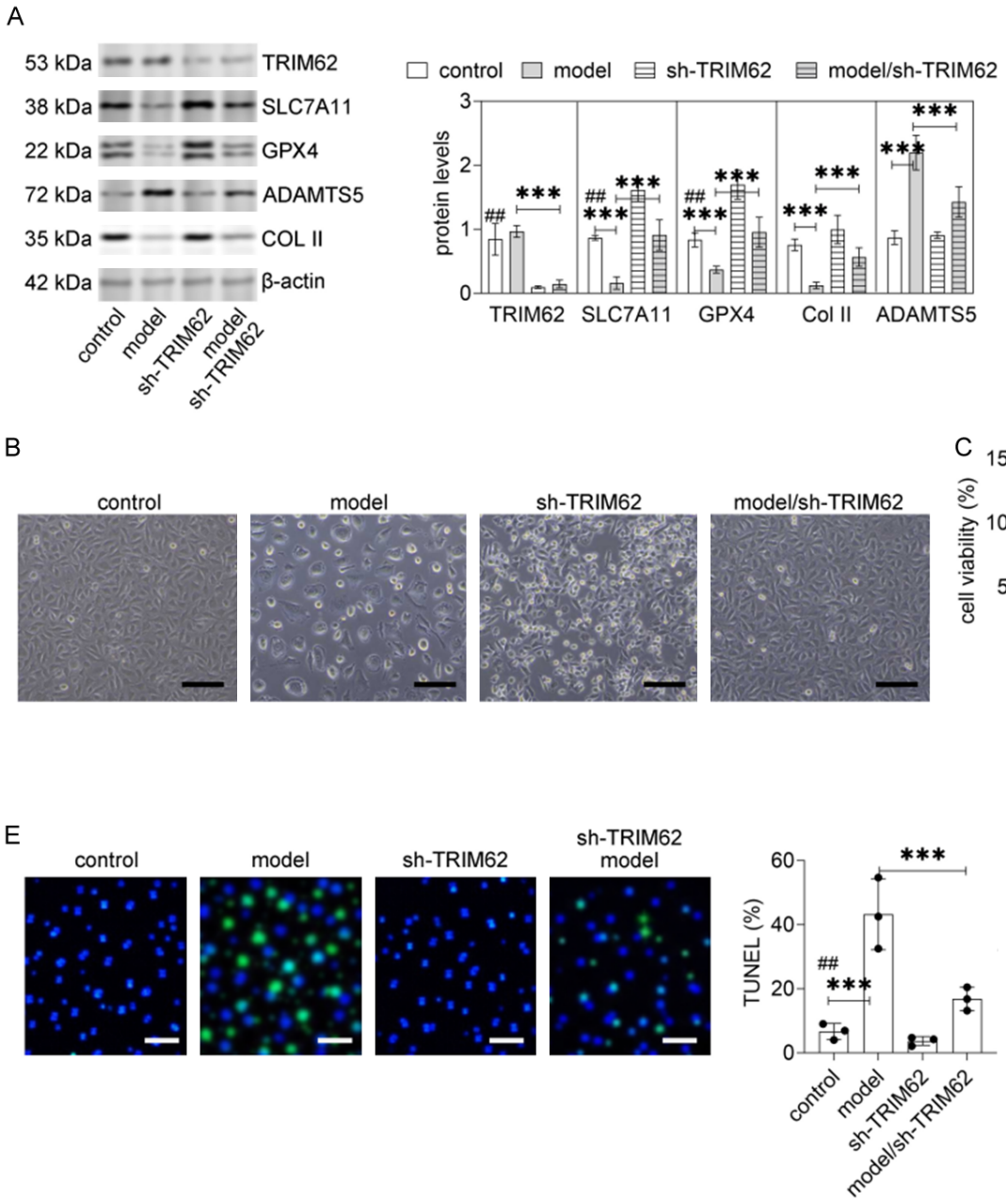
A
53 kDa
TRIM62
38 kDa
SLC7A11
22 kDa
GPX4
72 kDa
ADAMTS5
35 kDa
COL II
42 kDa
β-actin
control
model
sh-TRIM62
model
sh-TRIM62
control
model
sh-TRIM62
model/sh-TRIM62
protein levels
TRIM62
SLC7A11
GPX4
Col II
ADAMTS5
B
control
model
sh-TRIM62
model/sh-TRIM62
C
cell viability (%)
D
Fe2+ (μg/g)
E
control
model
sh-TRIM62
sh-TRIM62
model
TUNEL (%)

Figure 2. Knockdown of TRIM62 attenuates IL-1β-induced chondrocyte injury and ferroptosis. Primary rat chondrocytes were infected with sh-TRIM62 or sh-NC lentivirus, followed by treatment with IL-1β (10 ng/mL) or vehicle (PBS) for 24 h to establish the *in vitro* OA model. Cells were divided into four groups: control (sh-NC+PBS), model (sh-NC+IL-1β), sh-TRIM62 (sh-TRIM62+PBS), and model/sh-TRIM62 (sh-TRIM62+IL-1β) (n = 3 per group). A. Representative Western blot images and densitometric quantification of TRIM62, SLC7A11, GPX4, thrombospondin motifs 5 (ADAMTS5), and COL II protein expression. β-actin was used as the internal control. B. Morphological changes of chondrocytes were observed under a phase-contrast microscope. Scale bar = 100 μm. C. Cell viability was determined by the CCK-8 assay. D. Intracellular Fe^{2+} concentration was measured using an iron assay kit. E. Apoptosis was evaluated by TUNEL staining. Representative fluorescence images are shown on the left, with TUNEL-positive cells appearing green and nuclei counterstained with DAPI (blue). The percentage of TUNEL-positive cells was quantified and presented on the right. Scale bar = 50 μm. Data are presented as mean ± SD from three independent experiments. ***P < 0.001, connecting lines denote significant differences. #P < 0.05, ##P < 0.01, ###P < 0.001, sh-TRIM62 group versus control group.

findings demonstrate that TRIM62 promotes chondrocyte injury predominantly through ferroptosis rather than apoptosis or necroptosis.

TRIM62 interacts with GPX4 and promotes its proteasomal degradation

Having established that TRIM62 regulates ferroptosis in chondrocytes, we next sought to elucidate the underlying molecular mechanism. As an E3 ubiquitin ligase, TRIM62 may exert its effects by targeting key ferroptosis regulators for ubiquitination and degradation. We therefore investigated whether TRIM62 directly interacts with GPX4 or SLC7A11.

The outcomes of the Co-IP assay, conducted with an antibody targeting TRIM62, are illustrated in **Figure 4A**, GPX4 was readily detected in TRIM62 immunoprecipitates, whereas SLC7A11 was absent, indicating that TRIM62 specifically binds to GPX4 but not SLC7A11. Reciprocal Co-IP experiments confirmed this interaction: immunoprecipitation with anti-GPX4 antibody successfully pulled down TRIM62, while immunoprecipitation with anti-SLC7A11 antibody failed to precipitate TRIM62 (**Figure 4B**). Normal IgG served as a negative control and showed no detectable bands.

To determine whether TRIM62 promotes GPX4 degradation through the ubiquitin-proteasome pathway, we treated chondrocytes with the proteasome inhibitor MG132. Immunoblotting data indicated that the ectopic expression of TRIM62 led to a significant decline in the abundance of GPX4 protein. However, this reduction was completely abolished when cells were co-treated with MG132, indicating that TRIM62-mediated GPX4 downregulation depends on proteasomal activity (**Figure 4C**).

Immunofluorescence staining provided additional evidence supporting the TRIM62-GPX4 interaction. Double labelling showed that TRIM62 (red) and GPX4 (green) exhibited substantial co-localization in the cytoplasm of chondrocytes, as evidenced by yellow signals in merged images (**Figure 4D**). These results collectively demonstrate that TRIM62 physically interacts with GPX4 and promotes its degradation via the ubiquitin-proteasome pathway, thereby facilitating ferroptosis in chondrocytes.

TRIM62 knockdown alleviates cartilage damage and ferroptosis in vivo

To substantiate the cellular data within a biologically complex environment, we evaluated the remedial efficacy of TRIM62 silencing in a rat model of OA. sh-TRIM62 or sh-NC lentivirus was administered via intra-articular injection following ACLT surgery.

The elevated TRIM62 mRNA and protein levels observed in OA rats were substantially reduced in the OA/sh-TRIM62 group (P < 0.001; **Figure 5A**, **5B**). Importantly, TRIM62 knockdown restored the expression of SLC7A11 and GPX4 that had been suppressed in OA cartilage (P < 0.001; **Figure 5B**).

Histological assessment demonstrated that sh-TRIM62 treatment markedly attenuated OA-induced cartilage degeneration. Histological evaluation via H&E and SOFG staining demonstrated that the OA/sh-TRIM62 cohort possessed smoother articular surfaces, greater retention of the extracellular matrix (proteoglycans), and a more regular distribution of chondrocytes than the untreated OA group. These morphological improvements were mirrored by a substantial decline in OARSI scores among the rats receiving sh-TRIM62 (P < 0.001; **Figure 5C**).

Consistent with the histological improvements, ferroptosis markers were favorably modulated

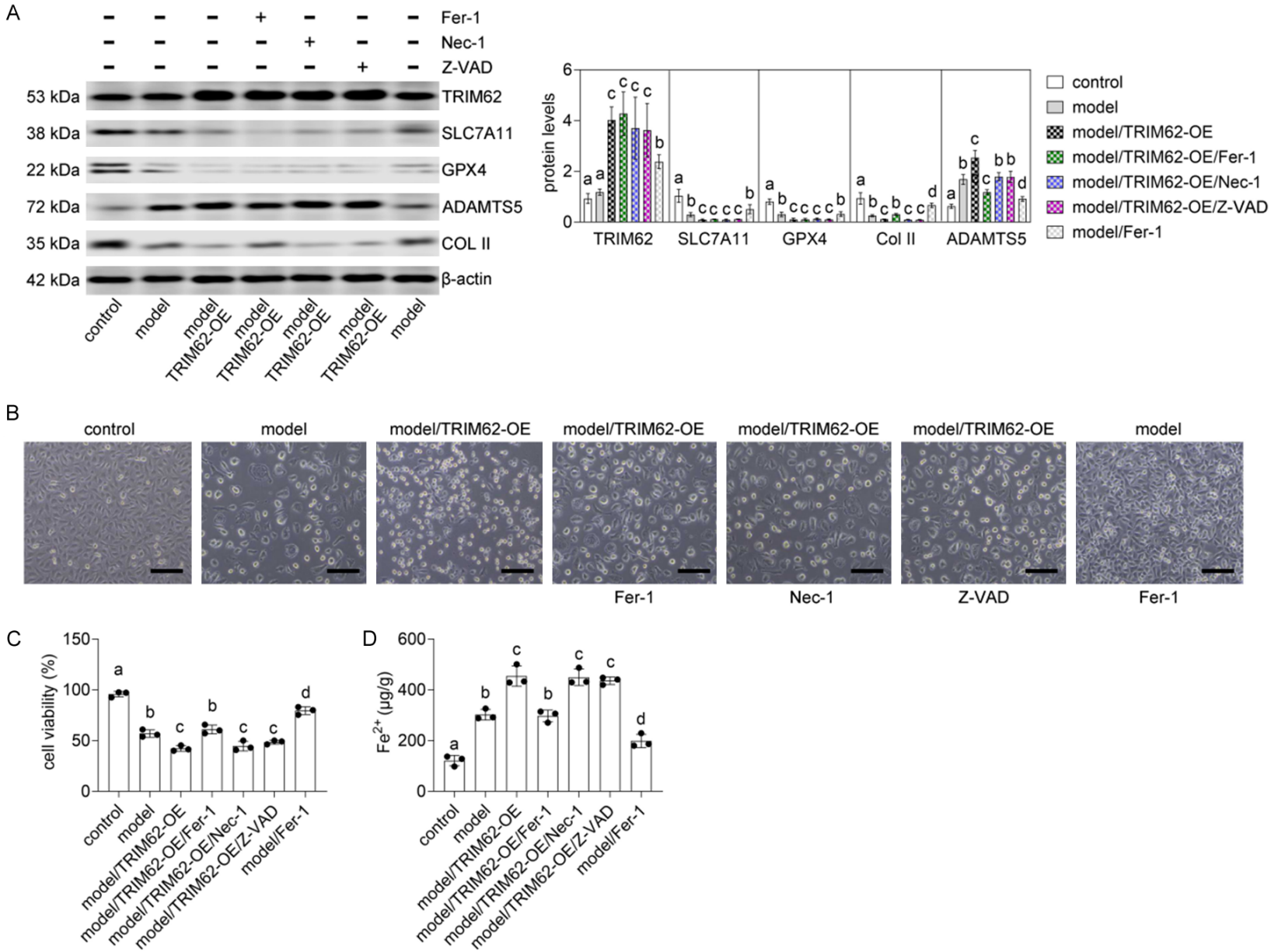
A
Fer-1
Nec-1
Z-VAD
53 kDa
TRIM62
38 kDa
SLC7A11
22 kDa
GPX4
72 kDa
ADAMTS5
35 kDa
COL II
42 kDa
β-actin
control
model
model TRIM62-OE
protein levels
TRIM62
SLC7A11
GPX4
Col II
ADAMTS5
control
model
model/TRIM62-OE
model/TRIM62-OE/Fer-1
model/TRIM62-OE/Nec-1
model/TRIM62-OE/Z-VAD
model/Fer-1
B
control
model
model/TRIM62-OE
Fer-1
Nec-1
Z-VAD
C
cell viability (%)
D
Fe2+ (μg/g)

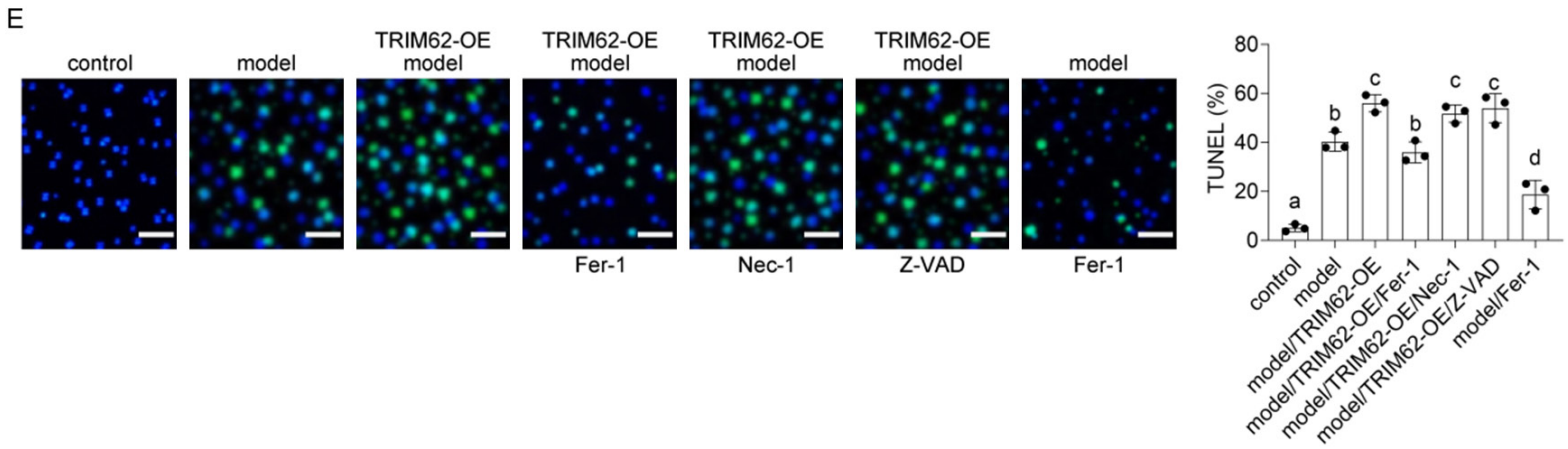

Figure 3. TRIM62 overexpression exacerbates chondrocyte injury through ferroptosis rather than apoptosis or necroptosis. Primary rat chondrocytes were transfected with the TRIM62 overexpression plasmid (TRIM62-OE) or empty vector, then stimulated with IL-1β (10 ng/mL) or vehicle (PBS) to induce the OA cell model. To determine the specific cell death pathway involved, cells were co-treated with the ferroptosis inhibitor Fer-1 (1 μM), the necroptosis inhibitor Nec-1 (30 μM), the apoptosis inhibitor Z-VAD (20 μM), or the corresponding vehicle (DMSO). Cells were divided into seven groups: control (empty vector + PBS + DMSO), model (empty vector+IL-1β+DMSO), model/TRIM62-OE (TRIM62-OE+IL-1β+DMSO), model/TRIM62-OE/Fer-1, model/TRIM62-OE/Nec-1, model/TRIM62-OE/Z-VAD, and model/Fer-1 (n = 3 per group). A. Western blot analysis and quantification of TRIM62, SLC7A11, GPX4, ADAMTS5, and COL II expression levels. β-actin served as the loading control. B. Representative phase-contrast microscopy images showing chondrocyte morphology. Scale bar = 100 μm. C. Cell viability was assessed using CCK-8 assay. D. Intracellular Fe^{2+} levels were quantified by an iron assay kit. E. Representative images of TUNEL staining (left) and quantification of TUNEL-positive cells (right). TUNEL-positive nuclei appear green, and total nuclei were counterstained with DAPI (blue). Scale bar = 50 μm. All data are expressed as mean ± SD from three independent experiments. Different lowercase letters indicate statistically significant differences between groups ($P < 0.05$); groups sharing the same letter are not significantly different.

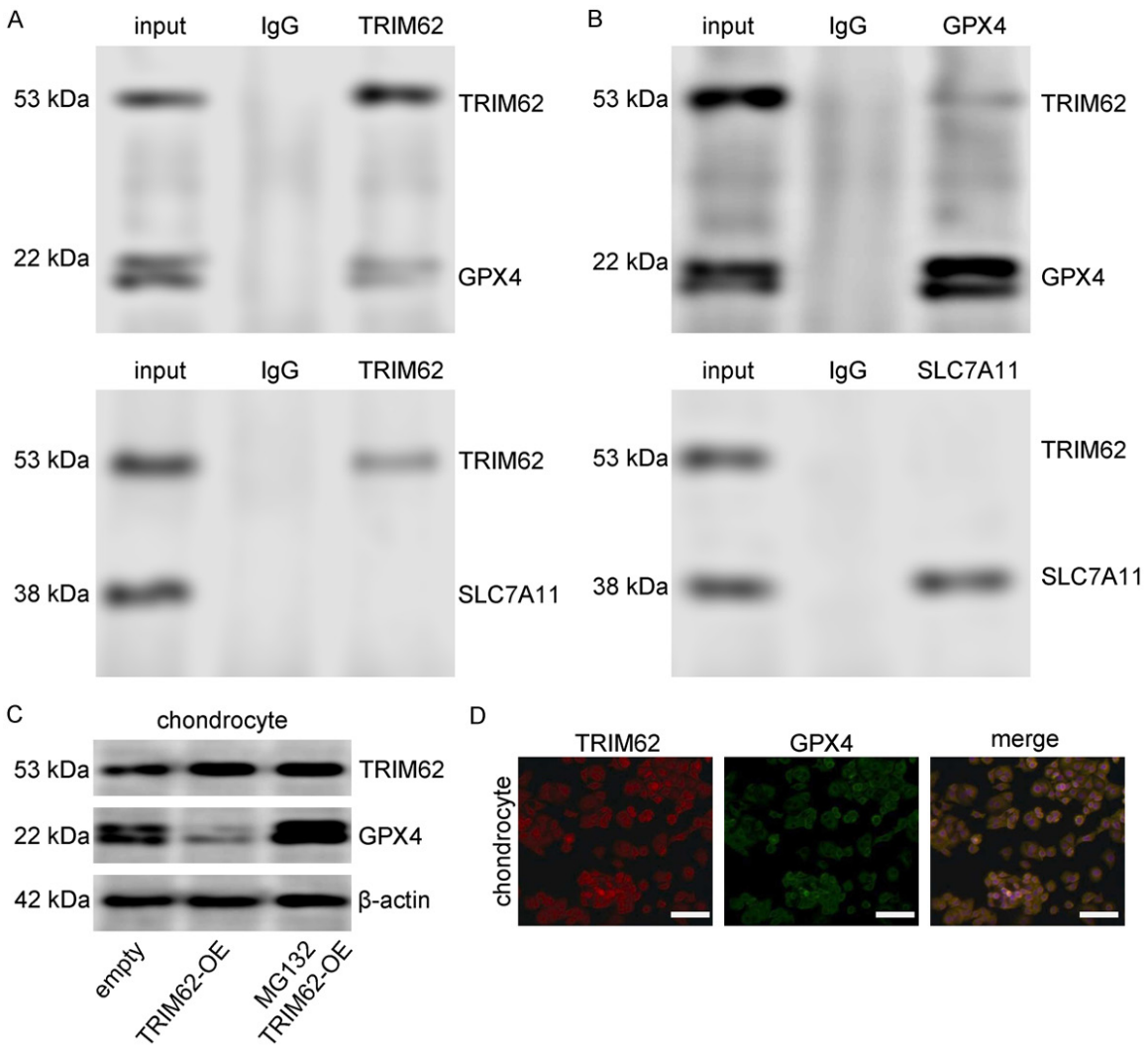

Figure 4. TRIM62 interacts with GPX4 but not SLC7A11 and promotes GPX4 protein degradation via the ubiquitin-proteasome pathway. Primary rat chondrocytes were used to investigate the interaction between TRIM62 and its potential substrates. A. Co-immunoprecipitation (Co-IP) analysis using anti-TRIM62 antibody. Cell lysates were immunoprecipitated with anti-TRIM62 antibody or normal IgG (negative control), and the immunoprecipitates were analyzed by immunoblotting for TRIM62, GPX4, and SLC7A11. Input represents 5% of total cell lysates. GPX4 was detected in TRIM62 immunoprecipitates, whereas SLC7A11 was not. B. Reciprocal Co-IP using anti-GPX4 or anti-SLC7A11 antibodies. TRIM62 was co-immunoprecipitated with GPX4 (upper panel) but not with SLC7A11 (lower panel), confirming the specific interaction between TRIM62 and GPX4. C. For proteasome inhibition experiments, chondrocytes were transfected with TRIM62-OE or empty vector, followed by treatment with MG132 (2.5 μM) or vehicle (DMSO) for 6 h. Cells were divided into four groups: empty vector+DMSO, TRIM62-OE+DMSO, empty vector+MG132, and TRIM62-OE+MG132. Western blot analysis of TRIM62 and GPX4 protein levels was performed. β-actin was used as the loading control. TRIM62 overexpression decreased GPX4 protein levels, which were reversed by MG132 treatment. D. Immunofluorescence staining showing subcellular co-localization of TRIM62 (red) and GPX4 (green) in chondrocytes. Yellow signals in merged images indicate co-localization of the two proteins in the cytoplasm. Scale bar = 50 μm.

by TRIM62 knockdown. Regarding antioxidant capacity, GSH concentrations were remarkably higher in the OA/sh-TRIM62 cohort than in the untreated OA model ($P < 0.001$; **Figure 5D**). Parallel to this, DCFH-DA assessments revealed that sh-TRIM62 treatment effectively curbed the buildup of reactive oxygen species (ROS) in diseased cartilage ($P < 0.001$; **Figure 5E**). Moreover, the dissipation of mitochondrial membrane potential - a hallmark of OA pathology - was significantly mitigated by TRIM62 silencing, as demonstrated by a notable increase in

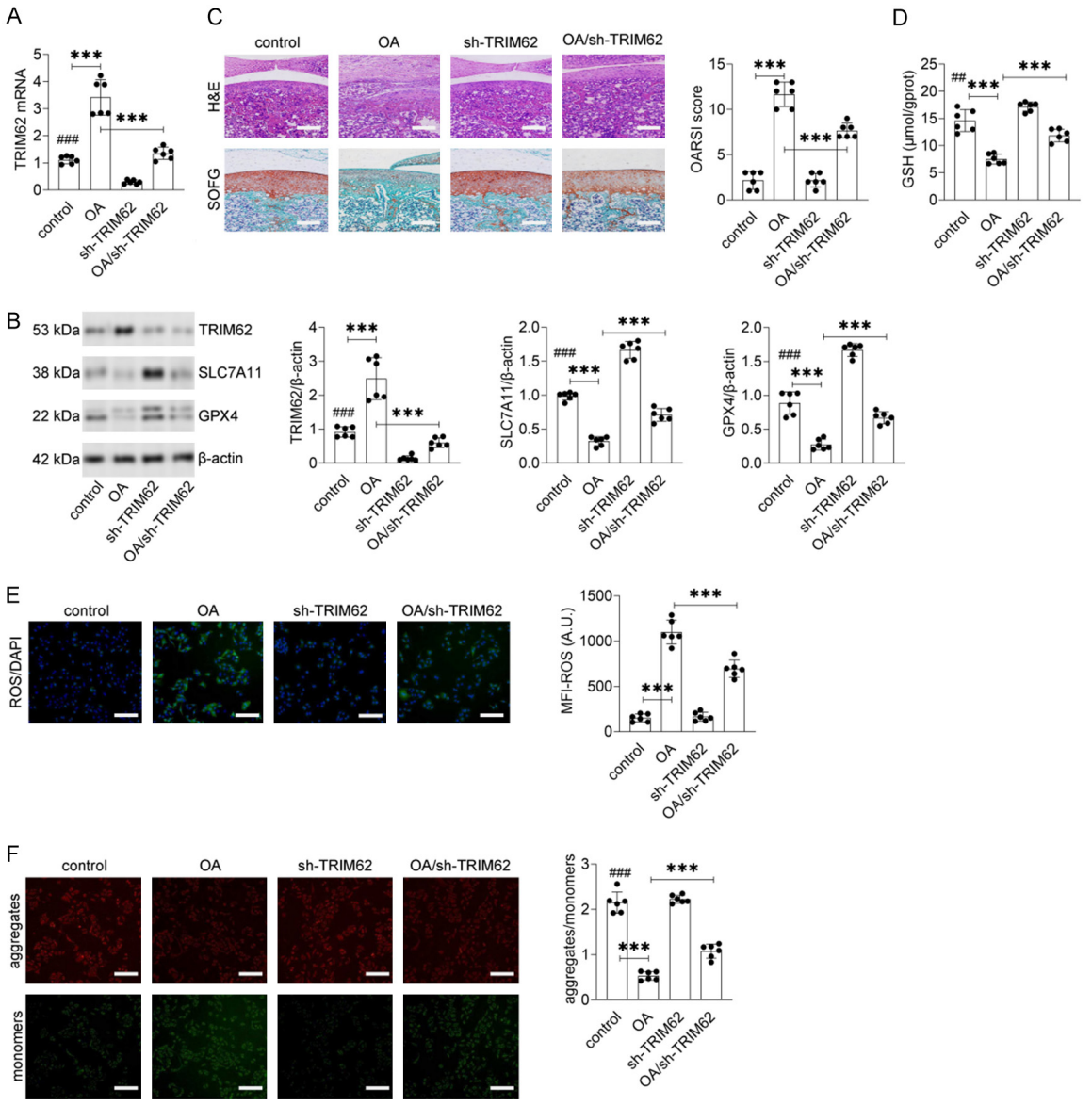

Figure 5. Knockdown of TRIM62 alleviates cartilage damage and ferroptosis *in vivo*. The OA rat model was established by anterior cruciate ligament transection (ACLT), while control rats underwent sham surgery. sh-TRIM62 or sh-NC lentivirus was administered via intra-articular injection. Rats were divided into four groups: control (sham+sh-NC), OA (ACLT+sh-NC), sh-TRIM62 (sham+sh-TRIM62), and OA/sh-TRIM62 (ACLT+sh-TRIM62) (n = 6 per group). Cartilage tissues were harvested 8 weeks post-surgery for analysis. A. Relative mRNA expression of TRIM62 in cartilage tissues was determined by RT-qPCR. B. Representative Western blot images and densitometric quantification of TRIM62, SLC7A11, and GPX4 protein levels. β-actin was used as the internal control. C. Histological evaluation of cartilage by hematoxylin and eosin (H&E) staining (upper panel) and safranin O-fast green (SOFG) staining (lower panel). Cartilage degradation severity was quantified using the OARSI scoring system (right). Scale bar = 100 μm. D. GSH concentration in cartilage tissues was measured by ELISA. E. ROS levels were assessed using DCFH-DA fluorescent probe. Representative images (left) and quantification of mean fluorescence intensity (MFI) (right) are shown. Nuclei were counterstained with DAPI (blue). Scale bar = 100 μm. F. Mitochondrial membrane potential was evaluated by JC-1 staining. Red fluorescence indicates JC-1 aggregates (intact membrane potential), while green fluorescence represents JC-1 monomers (depolarized mitochondria). The ratio of aggregates to monomers was calculated and is presented in the bar graph. Scale bar = 100 μm. Data are expressed as mean ± SD. ***P < 0.001, connecting lines denote significant differences. ##P < 0.01, ###P < 0.001, sh-TRIM62 group versus control group.

the red-to-green fluorescence ratio during JC-1 analysis (P < 0.001; **Figure 5F**). These *in vivo* data provide strong evidence that targeting TRIM62 effectively mitigates OA progression by

suppressing ferroptosis and preserving cartilage integrity.

Discussion

The present study provides comprehensive evidence demonstrating that TRIM62 is significantly upregulated in OA cartilage and promotes disease progression by facilitating GPX4 ubiquitination and degradation, thereby triggering chondrocyte ferroptosis. Several lines of evidence support this conclusion. Our findings revealed a distinct pathological pattern where significant TRIM62 upregulation occurred in parallel with a decline in GPX4 and SLC7A11 abundance across both rat OA specimens and IL-1β-challenged chondrocytes. Our functional evaluations indicated that the depletion of TRIM62 served a protective role against IL-1β-triggered damage and ferroptosis, while its upward modulation further aggravated these pathological insults. Crucially, the cytotoxic impact of TRIM62 was uniquely neutralized by the ferroptosis-specific blocker ferrostatin-1, whereas inhibitors targeting apoptosis (Z-VAD-FMK) or necroptosis (necrostatin-1) showed no such remedial effect. This specificity confirms that TRIM62-mediated chondrocyte demise is executed primarily via the ferroptotic pathway. From a mechanistic perspective, we identified that TRIM62 physically associates with GPX4 to facilitate its proteasomal degradation, whereas the expression of SLC7A11 remains unaffected by this interaction. These findings collectively establish the TRIM62-GPX4-ferroptosis axis as a novel pathogenic mechanism in OA.

Ferroptosis has emerged as a critical contributor to OA pathogenesis in recent years. Pioneering work demonstrated that ferroptotic hallmarks, including iron accumulation, lipid peroxidation, and GPX4 downregulation, are prominent features of human OA cartilage [31]. Further investigations have established that ferroptotic cell death is a critical component of the chondrocytic response to various OA-inducing insults, most notably pro-inflammatory cytokines, excessive physical loading, and redox stress [31]. Evidence suggests that abnormal physical loading precipitates a GPX4-dependent ferroptotic process in cartilage cells, which is fundamentally driven by calcium mobilization through the Piezo1 mechanoreceptor [32]. Similarly, our findings are consistent with these reports, as we observed reduced GPX4 expression, decreased GSH levels, elevated intracellular iron and ROS levels, and impaired mitochondrial membrane potential in OA cartilage. Furthermore, treatment with ferrostatin-1 effectively rescued chondrocyte viability and preserved ECM homeostasis, reinforcing the notion that ferroptosis represents a druggable target in OA. Our study extends these findings by identifying TRIM62 as an upstream regulator that initiates the ferroptotic cascade through destabilizing GPX4.

GPX4 occupies a central position in the ferroptosis regulatory network by serving as the primary enzyme that detoxifies lipid hydroperoxides [33]. Genetic ablation of GPX4 leads to embryonic lethality in mice, and conditional knockout of GPX4 in specific tissues results in tissue damage characterized by ferroptotic features [34]. In the context of OA, Wang et al. demonstrated that GPX4 conditional knockout mice exhibited accelerated cartilage degeneration following destabilization of the medial meniscus surgery [32]. Apart from its conventional function in preventing lipid-based oxidative damage, GPX4 is increasingly recognized for its contribution to extracellular matrix (ECM) homeostasis in chondrocytes. Previous literature suggests that a deficiency in GPX4 not only heightens cellular vulnerability to redox imbalance but also worsens the depletion of the matrix by triggering the MAPK/NF-κB signaling cascade [1]. Our results noted that the degradation of GPX4 mediated by TRIM62 coincided with suppressed COL II synthesis and heightened ADAMTS5 levels, highlighting a regulatory connection between ferroptotic death and matrix degradation. The multifaceted role of GPX4 in managing lipid stability and preserving ECM homeostasis positions it as a promising focal point for the development of novel OA therapies.

Post-translational regulation of GPX4 through ubiquitination has gained considerable attention in ferroptosis research. Several E3 ubiquitin ligases have been identified as modulators of GPX4 protein stability. Wang et al. reported that TRIM26 binds K63-linked ubiquitin chains on GPX4, which paradoxically stabilizes GPX4 and protects glioma cells from ferroptosis [25]. In contrast, studies demonstrated that TRIM25 mediates K48-linked ubiquitination of GPX4 in pancreatic cancer cells, promoting GPX4 degradation and rendering cells sus-

ceptible to ferroptotic death [26]. The divergent outcomes of GPX4 ubiquitination highlight the importance of ubiquitin chain topology in determining protein fate. The biological fate of a protein is largely dictated by its ubiquitin linkage type: while K48-tethered ubiquitin polymers primarily serve as signals for 26S proteasome-mediated destruction, K63-linked chains predominantly participate in non-proteolytic processes, including the modulation of signaling cascades, subcellular trafficking, and protein activity [24, 34]. Our findings align with the K48-ubiquitination model, as TRIM62-induced GPX4 downregulation was completely reversed by the proteasome inhibitor MG132, indicating that TRIM62 promotes GPX4 degradation through the ubiquitin-proteasome pathway. Future studies employing ubiquitination site mapping and linkage-specific ubiquitin antibodies will be valuable for precisely characterizing the ubiquitin chain type mediated by TRIM62.

An intriguing finding of our study is that TRIM62 specifically interacts with GPX4 but not SLC7A11, despite both being key components of the ferroptosis defense machinery. Co-immunoprecipitation experiments clearly demonstrated that TRIM62 forms a complex with GPX4, whereas no interaction was detected between TRIM62 and SLC7A11. This substrate selectivity is consistent with the structural basis of E3 ligase-substrate recognition, which typically involves specific protein-protein interaction domains and motifs [35]. Notably, other TRIM family members exhibit different substrate preferences in the ferroptosis pathway. TRIM7 has been shown to target SLC7A11 for K48-linked ubiquitination in gastric cancer cells, leading to SLC7A11 degradation and ferroptosis induction [27]. In the pathological context of non-small cell lung cancer, TRIM3 has been shown to facilitate the K11-specific polyubiquitination of SLC7A11, ultimately leading to its proteolytic breakdown [36]. The distinct substrate specificities of different TRIM proteins suggest that multiple E3 ligases cooperate to fine-tune ferroptosis sensitivity by targeting different nodes of the ferroptosis regulatory network. In OA, we observed concurrent downregulation of both SLC7A11 and GPX4; however, only GPX4 is directly targeted by TRIM62. The reduction in SLC7A11 expression may represent a secondary consequence of GPX4 loss or result from regulation by other mechanisms, such as transcriptional repression or degradation mediated by alternative E3 ligases [27].

The potential cross-talk between ferroptotic cell death and matrix metabolism in chondrocytes is a subject of significant interest. The steady state of the ECM is traditionally governed by the dynamic competition between anabolic molecules and matrix-degrading enzymes [37, 38]. In OA, this equilibrium is disrupted, leading to progressive cartilage degradation [38]. Our results demonstrated that TRIM62 knockdown not only suppressed ferroptosis markers but also restored collagen type II expression while reducing ADAMTS5 levels. Conversely, TRIM62 overexpression exacerbated ECM catabolism, which was partially reversed by ferrostatin-1 treatment. These observations suggest that ferroptosis and ECM degradation are mechanistically linked in OA chondrocytes. One possible explanation is that ferroptosis-induced oxidative stress activates catabolic signaling pathways, such as NF-κB and MAPK, which in turn upregulate matrix-degrading enzymes [39]. Additionally, iron accumulation during ferroptosis may directly enhance the activity of iron-dependent matrix metalloproteinases [40]. The intricate biochemical bridges linking ferroptotic cell death to the metabolic turnover of the ECM are not yet fully charted, indicating a fertile territory for upcoming scientific inquiry.

With a focus on drug development, the current findings suggest that the TRIM62/GPX4/ferroptosis axis represents a viable focal point for OA intervention. Various approaches could be implemented to exploit this mechanism. Specifically, pharmacological suppression of TRIM62 E3 ligase activity would prevent the depletion of GPX4 protein and consequently inhibit the initiation of ferroptotic chondrocyte death [29]. Alternatively, stabilization of GPX4 through inhibition of the ubiquitin-proteasome system or through the development of GPX4-protecting agents could achieve similar outcomes. Direct supplementation with ferroptosis inhibitors, such as ferrostatin-1 or liproxstatin-1, has shown protective effects in preclinical OA models [41]. Iron chelators, including deferoxamine, have also demonstrated cartilage-protective effects by reducing iron-mediated lipid peroxidation [42]. The development of chondrocyte-targeted delivery systems for these therapeutic

agents would enhance their efficacy while minimizing systemic side effects [43]. Furthermore, natural compounds with anti-ferroptotic properties, such as astragaloside IV and icariin, have shown promising effects in alleviating OA by modulating the SLC7A11/GPX4 axis [44]. Combination therapies targeting multiple nodes of the ferroptosis pathway may offer synergistic benefits.

The scope of this study is subject to several caveats. Primarily, our mechanistic insights were garnered from rat-derived chondrocytes and *in vivo* models, meaning the direct extrapolation of these data to human pathology requires caution. Future efforts to validate the role of TRIM62 in human osteoarthritic samples will be crucial for confirming the cross-species relevance of our laboratory observations. Although we demonstrated the interaction between TRIM62 and GPX4, the precise binding interface and ubiquitination sites on GPX4 remain to be determined through structural and mass spectrometry analyses. The upstream regulators of TRIM62 expression in OA, including inflammatory cytokines, mechanical stress, and epigenetic modifications, were not explored in this study. Additionally, although we established that TRIM62 promotes ferroptosis by degrading GPX4, we cannot exclude the possibility that it targets other substrates that contribute to OA pathogenesis. Future studies employing proteomics approaches to identify the complete TRIM62 substratome in chondrocytes would provide a more comprehensive understanding of its biological functions. Finally, the development of selective TRIM62 inhibitors and their evaluation in clinically relevant OA models would be essential for translating our findings into therapeutic applications.

In conclusion, this study identifies TRIM62 as a novel regulator of chondrocyte ferroptosis in OA. We demonstrate that TRIM62 is upregulated in OA cartilage and promotes GPX4 ubiquitination and degradation, thereby triggering ferroptotic cell death and accelerating cartilage degeneration. Targeting the TRIM62-GPX4 axis may offer new therapeutic opportunities for OA intervention. These findings advance our understanding of the molecular mechanisms underlying OA pathogenesis and highlight ferroptosis as a therapeutic target in degenerative joint diseases.

Conclusion

In conclusion, our findings demonstrate that TRIM62 promotes OA progression by facilitating the ubiquitination and degradation of GPX4, thereby triggering chondrocyte ferroptosis. Targeting the TRIM62-GPX4-ferroptosis axis represents a promising therapeutic strategy for OA treatment.

Acknowledgements

This study was supported by the National Natural Science Foundation of China (Grant No. 82172439).

Disclosure of conflict of interest

None.

Address correspondence to: Yonghong Zhang, Department of Orthopaedics, Second Hospital of Shanxi Medical University, No. 382 Wuyi Road, Xinghualing District, Taiyuan 030001, Shanxi, China. E-mail: yhzhy@sxmu.edu.cn

References

[1] Li H, Chen P, Cheng W, Zhang Z, Yang J, Zhang H, Jin F, Kan L, Chen L and Wang H. Programmed cell death in osteoarthritis. Apoptosis 2026; 31: 3.

[2] Wang Y, Tang X, Peng JR, Deng Y, Lan S, Yen Y and Tang Y. Global, regional, and national burden of osteoarthritis among middle-aged and older adults: estimates from the global burden of disease study 2021 and projections to 2050. Front Med (Lausanne) 2025; 12: 1696929.

[3] Hunter DJ and Eckstein F. Exercise and osteoarthritis. J Anat 2009; 214: 197-207.

[4] Yucesoy B, Charles LE, Baker B and Burchfiel CM. Occupational and genetic risk factors for osteoarthritis: a review. Work 2015; 50: 261-273.

[5] Huang K and Cai H. The role of chondrocyte senescence in osteoarthritis pathogenesis and therapeutic implications. Exp Gerontol 2025; 208: 112828.

[6] Mei J, Xiao N, Xi Y, Chen X, Zha X, Cui L, Yan F, Xue R, Wang Y and Ma Y. Regulation of apoptosis and interaction with cartilage degeneration in osteoarthritis. Front Cell Dev Biol 2025; 13: 1571448.

[7] Hao W, Chang M, Shi D, Yun C, Li J, Guo H and Lin X. Therapeutic targets in aging-related osteoarthritis: a focus on the extracellular matrix homeostasis. Life Sci 2025; 368: 123487.

[8] Guo Z, Qu Z, Zhang Y, Xu D, Chu L and Cheng M. Effects and mechanisms of MSCs and MSC-derived exosomes in regulating ferroptosis. J Physiol Biochem 2025; 81: 1001-1018.
[9] Duo K, Feng X, Tian X, Wang F, Zhao Y, Yu J, Liu Y, He Y and Cai Z. Ferroptosis inhibitors: mechanisms of action and therapeutic potential. Cell Mol Life Sci 2025; 82: 441.
[10] Pham J, Refesse M, Saeed A and Latunde-Dada GO. Haem oxygenase-1, ferroptosis and disorders-a narrative review. Nutrients 2025; 17: 3921.
[11] He Y, Wang J, Ying C, Xu KL, Luo J, Wang B, Gao J, Yin Z and Zhang Y. The interplay between ferroptosis and inflammation: therapeutic implications for cerebral ischemia-reperfusion. Front Immunol 2024; 15: 1482386.
[12] Feng H, Schorpp K, Jin J, Yozwiak CE, Hoffstrom BG, Decker AM, Rajbhandari P, Stokes ME, Bender HG, Csuka JM, Upadhyayula PS, Canoll P, Uchida K, Soni RK, Hadian K and Stockwell BR. Transferrin receptor is a specific ferroptosis marker. Cell Rep 2020; 30: 3411-3423, e3417.
[13] Chang X, Kang Y, Yang Y, Chen Y, Shen Y, Jiang C and Shen Y. Pyroptosis: a novel intervention target in the progression of osteoarthritis. J Inflamm Res 2022; 15: 3859-3871.
[14] Yazar M, Sarban S, Kocyigit A and Isikan UE. Synovial fluid and plasma selenium, copper, zinc, and iron concentrations in patients with rheumatoid arthritis and osteoarthritis. Biol Trace Elem Res 2005; 106: 123-132.
[15] Stockwell BR, Friedmann Angeli JP, Bayir H, Bush AI, Conrad M, Dixon SJ, Fulda S, Gascón S, Hatzios SK, Kagan VE, Noel K, Jiang X, Linkermann A, Murphy ME, Overholtzer M, Oyagi A, Pagnussat GC, Park J, Ran Q, Rosenfeld CS, Salnikow K, Tang D, Torti FM, Torti SV, Toyokuni S, Woerpel KA and Zhang DD. Ferroptosis: a regulated cell death nexus linking metabolism, redox biology, and disease. Cell 2017; 171: 273-285.
[16] Ansari MY, Ahmad N and Haqqi TM. Oxidative stress and inflammation in osteoarthritis pathogenesis: role of polyphenols. Biomed Pharmacother 2020; 129: 110452.
[17] Dixon SJ, Lemberg KM, Lamprecht MR, Skouta R, Zaitsev EM, Gleason CE, Patel DN, Bauer AJ, Cantley AM, Yang WS, Morrison B 3rd and Stockwell BR. Ferroptosis: an iron-dependent form of nonapoptotic cell death. Cell 2012; 149: 1060-1072.
[18] Zou K, Liu W, Xia W and Zhao Y. Ferroptosis in hypertriglyceridemic acute pancreatitis: mechanisms and therapeutic implications. J Inflamm Res 2025; 18: 18115-18135.
[19] Dai Q, Wei X, Zhao J, Zhang D, Luo Y, Yang Y, Xiang Y and Liu X. Inhibition of FSP1: a new strategy for the treatment of tumors (Review). Oncol Rep 2024; 52: 105.
[20] Yang Q, Zhao J, Chen D and Wang Y. E3 ubiquitin ligases: styles, structures and functions. Mol Biomed 2021; 2: 23.
[21] Zheng N and Shabek N. Ubiquitin ligases: structure, function, and regulation. Annu Rev Biochem 2017; 86: 129-157.
[22] Di Rienzo M, Zuchegna C, Perri V, Piacentini M, Falasca L and Romagnoli A. The role of TRIM proteins in the pathogenesis of mycobacterium tuberculosis. Biol Direct 2025; 21: 1.
[23] Wang J, Wang Q, Li X, Cai Q, Bi Y, Xu C, Bai H, Gu L, Chang G and Chen S. Emerging roles of TRIM in metabolic regulation. Metabolism 2026; 174: 156394.
[24] Livshits G and Kalinkovich A. The role of TRIM proteins in chronic inflammation-associated musculoskeletal diseases. Ageing Res Rev 2025; 111: 102837.
[25] Wang Z, Xia Y, Wang Y, Zhu R, Li H, Liu Y and Shen N. The E3 ligase TRIM26 suppresses ferroptosis through catalyzing K63-linked ubiquitination of GPX4 in glioma. Cell Death Dis 2023; 14: 695.
[26] Wang HJ, Dong LF, Ding LL, Miao XY, Zhang YW, Zhao LP, Yu LH, Guan ZR, Jiang YP, Tang XQ, Yan YX and Lou JS. TFEB promotes Ginkgetin-induced ferroptosis via TRIM25 mediated GPX4 lysosomal degradation in EGFR wide-type lung adenocarcinoma. Theranostics 2025; 15: 2991-3012.
[27] Chen Q, Zhang T, Zeng R, Zhang K, Li B, Zhu Z, Ma X, Zhang Y, Li L, Zhu J and Zhang G. The E3 ligase TRIM7 suppresses the tumorigenesis of gastric cancer by targeting SLC7A11. Sci Rep 2024; 14: 6655.
[28] Huang LY, Liu YN, Li LL, Zhang MN, Miao XY, Liang ZY, Sun B, Su RQ, Qin ZL, Wen ZF, Wang W, Shen JG and Qi SH. Momordica charantia small extracellular vesicles mitigate neuronal ferroptosis by inhibition of GPX4 ubiquitination in ischemic stroke. Phytomedicine 2025; 148: 157298.
[29] Huang F, Xiao H, Sun BL and Yang RG. Characterization of TRIM62 as a RING finger E3 ubiquitin ligase and its subcellular localization. Biochem Biophys Res Commun 2013; 432: 208-213.
[30] Li P, Xu TY, Yu AX, Liang JL, Zhou YS, Sun HZ, Dai YL, Liu J and Yu P. The role of ferroptosis in osteoporosis and advances in Chinese herbal interventions. Biology (Basel) 2025; 14: 367.
[31] Xu W, Zhang B, Xi C, Qin Y, Lin X, Wang B, Kong P and Yan J. Ferroptosis plays a role in human chondrocyte of osteoarthritis induced by IL-1β in vitro. Cartilage 2023; 14: 455-466.
[32] Wang S, Li W, Zhang P, Wang Z, Ma X, Liu C, Vasilev K, Zhang L, Zhou X, Liu L, Hayball J,

Dong S, Li Y, Gao Y, Cheng L and Zhao Y. Mechanical overloading induces GPX4-regulated chondrocyte ferroptosis in osteoarthritis via Piezo1 channel facilitated calcium influx. J Adv Res 2022; 41: 63-75.
[33] Qian JY, Lou CY, Chen YL, Ma LF, Hou W and Zhan ZJ. A prospective therapeutic strategy: GPX4-targeted ferroptosis mediators. Eur J Med Chem 2025; 281: 117015.
[34] Park S, Park MJ, Kwon EJ, Oh JY, Chu YJ, Kim HS, Park S, Kim TH, Kwon SW, Kim YS and Cha HJ. The protective role of GPX4 in naïve ESCs is highlighted by induced ferroptosis resistance through GPX4 expression. Redox Biol 2025; 81: 103539.
[35] Uljon S, Xu X, Durzynska I, Stein S, Adelmant G, Marto JA, Pear WS and Blacklow SC. Structural basis for substrate selectivity of the E3 ligase COP1. Structure 2016; 24: 687-696.
[36] Wang Z, Shen N, Wang Z, Yu L, Yang S, Wang Y, Liu Y, Han G and Zhang Q. TRIM3 facilitates ferroptosis in non-small cell lung cancer through promoting SLC7A11/xCT K11-linked ubiquitination and degradation. Cell Death Differ 2024; 31: 53-64.
[37] Sun W, Zhou S, Peng L, Wang W, Liu Y, Wang T, Cheng D, Li Z, Xiong H, Jia X, Lian W, Jiao J and Ni C. Fatty acid oxidation-glycolysis metabolic transition affects ECM homeostasis in silica-induced pulmonary fibrosis. Adv Sci (Weinh) 2025; 12: e2407134.
[38] Ashruf OS and Ansari MY. Natural compounds: potential therapeutics for the inhibition of cartilage matrix degradation in osteoarthritis. Life (Basel) 2022; 13: 102.
[39] Zhao C, Sun G, Li Y, Kong K, Li X, Kan T, Yang F, Wang L and Wang X. Forkhead box O3 attenuates osteoarthritis by suppressing ferroptosis through inactivation of NF-κB/MAPK signaling. J Orthop Translat 2023; 39: 147-162.
[40] Abdukarimov N, Kokabi K and Kunz J. Ferroptosis and iron homeostasis: molecular mechanisms and neurodegenerative disease implications. Antioxidants (Basel) 2025; 14: 527.
[41] Liu Y, Zhang Z, Fang Y, Liu C and Zhang H. Ferroptosis in osteoarthritis: current understanding. J Inflamm Res 2024; 17: 8471-8486.
[42] Wang H, Zhou Z, Wu T, Fan Z, Jin Z, Cao Y, Huangfu C, Wang Y, Liu X and Liu D. Deferoxamine improves intervertebral disc degeneration by activating HIF-1α/BNIP3-mediated mitophagy and inhibiting ferroptosis. Int Immunopharmacol 2025; 166: 115583.
[43] Moradi M, Najibi A, Moshfeghinia R, Heidarian A, Moradi M and Fehlings MG. The role of the iron-chelating agent deferoxamine in spinal cord injury: a systematic review and meta-analysis of preclinical studies. Spine J 2026; 26: 239-251.
[44] Yang K, Xie Q, Tang T, Zhao N, Liang J, Shen Y, Li Z, Liu B, Chen J, Cheng W, Bai X, Zhang P, Liu Q, Song B, Hu C, Liu L and Wang Y. Astragaloside IV as a novel CXCR4 antagonist alleviates osteoarthritis in the knee of monosodium iodoacetate-induced rats. Phytomedicine 2023; 108: 154506.